Monthly Notices of the ROYAL ASTRONOMICAL SOCIETY

MNRAS **497,** 94–108 (2020) doi:10.1093/mnras/staa1840
Advance Access publication 2020 June 27

Optical spectroscopy of BL Lac objects: TeV candidates

Simona Paiano [1,2,3★] Renato Falomo [4], Aldo Treves[3,5] and Riccardo Scarpa[6,7]

[1]*INAF – Osservatorio Astronomico di Roma, via Frascati 33, I-00040 Monteporzio Catone, Italy*
[2]*INAF – IASF Milano, via Corti 12, I-20133 Milano, Italy*
[3]*Università dell'Insubria, Dipartimento di Scienza e Alta Tecnologia (DISAT), via Valleggio 11, I-22100, Como, Italy*
[4]*INAF – Osservatorio Astronomico di Padova, vicolo dell'Osservatorio 5, I-35122 Padova, Italy*
[5]*INAF – Osservatorio Astronomico di Brera, via Bianchi 46, I-23807 Merate (Lecco), Italy*
[6]*Instituto de Astrofisica de Canarias, C/O Via Lactea s/n, E-38205 La Laguna, Tenerife, Spain*
[7]*Departamento de Astrofísica, Universidad de La Laguna, E-38206 La Laguna, Tenerife, Spain*

Accepted 2020 June 22. Received 2020 June 22; in original form 2020 April 13

ABSTRACT

We investigate the spectroscopic optical properties of gamma-ray sources detected with high significance above 50 GeV in the Third Catalog of Hard *Fermi*-LAT Sources and that are good candidates as TeV emitters. We focus on the 91 sources that are labelled by the *Fermi* team as BL Lac (BLL) objects or blazar candidates of uncertain type (BCUs), are in the Northern hemisphere, and are with unknown or uncertain redshift. We report here on GTC (Gran Telescopio Canarias) spectra (in the spectral range 4100–7750 Å) of 13 BCUs and 42 BLL objects. We are able to classify the observed targets as BLL objects and each source is briefly discussed. The spectra allowed us to determine the redshift of 25 objects on the basis of emission and/or absorption lines, finding $0.05 < z < 0.91$. Most of the emission lines detected are due to forbidden transition of [O III] and [N II]. The observed line luminosity is found to be lower than that of quasi-stellar objects (QSOs) at similar continuum and could be reconciled with the line–continuum luminosity relationship of QSOs if a significant beaming factor is assumed. Moreover, for five sources we found intervening absorption lines that allow to set a spectroscopic lower limit of the redshift. For the remaining 25 sources, for which the spectra are lineless, a lower limit to z is given, assuming that the host galaxies are giant ellipticals.

Key words: galaxies: active – BL Lacertae objects: general – gamma-rays: galaxies.

1 INTRODUCTION

BL Lac (BLL) objects are active galactic nuclei (AGNs), whose emission is dominated by non-thermal radiation from a relativistically beamed jet aligned with the line of sight. The emission, of synchrotron-inverse Compton origin, extends over the whole electromagnetic spectrum, from radio to gamma-ray. Distinctive characteristics of the class are the large and rapid flux variability, high polarization, and the absence or weakness of spectral lines, washed out by the emission from the jet, which in most cases makes very arduous the determination of their distance.

Data sets of BLL objects have been produced through a number of dedicated surveys in all spectral bands, originally in the radio (Stickel et al. 1991; Giommi et al. 2002; Marchã & Caccianiga 2013) and X-rays (Stocke et al. 1990; Perlman et al. 1996, 1998; Laurent-Muehleisen et al. 1998, 1999; Voges et al. 1999; Cusumano et al. 2010), then in the optical and infrared (IR; e.g. Falomo et al. 2000; Scarpa et al. 2000a,b; Urry et al. 2000; Plotkin et al. 2010; D'Abrusco et al. 2014, 2019), and more recently also in the gamma-ray band (Abdollahi et al. 2020, and references in therein). The latter surveys indeed showed that BLL objects represent the dominant extragalactic population of gamma sources (*Fermi*-LAT Collaboration 2019). Thanks to its systematic monitoring of the whole sky, and the long duration of the mission, the *Fermi* catalogues of gamma-ray sources have become a privileged means for discovering new BLL objects. The procedure of identification of the counterpart of the gamma-ray emitter generally goes through the search of X-ray and radio sources in the gamma-ray error box (e.g. Stephen et al. 2010; Takeuchi et al. 2013; Landi et al. 2015; Paiano, Franceschini & Stamerra 2017a). The BLL nature of the target can be guessed because of the broad spectral energy distribution, which in a BLL object is well characterized by two broad humps, one due to synchrotron radiation (IR–optical) and the other due to inverse Compton scattering (X-rays to gamma-rays; see e.g. Maraschi, Ghisellini & Celotti 1992; Ghisellini & Tavecchio 2009; Madejski & Sikora 2016; Ghisellini et al. 2017). However, the secure classification derives generally from optical spectroscopy. The identification of weak spectral lines is the basic tool for obtaining first of all a firm classification and the distance of the source, but also for constraining some physical parameters of the emission region. If no intrinsic lines are observed, there are indirect procedures based on some hypothesis on the nature of the host galaxy, which can effectively produce lower limit to the redshift of the source (e.g. Sbarufatti et al. 2006a,b; Meisner & Romani 2010; Falomo, Pian & Treves 2014; see also Section 4). In some cases, the optical spectra can exhibit absorption lines due to intervening medium, from which a spectroscopic lower limit to z can be derived.

★ E-mail: simona.paiano@inaf.it

The knowledge of the distance is a basic ingredient for modelling the BLL objects, for constructing the luminosity function of this class of blazars, for assessing the cosmic evolution, and for evaluating the contribution of the BLL population to the gamma-ray cosmic background. Because the overall spectrum may extend to the TeV domain, BLL objects of known redshift are unique probes of the extragalactic background light (EBL), since at $z \geq 1$ the absorption effects due to pair production become important (Franceschini et al. 2017). Some BLL objects are also supposedly ultrahigh-energy (PeV) neutrino emitters (Ahlers & Halzen 2015; Padovani et al. 2016; Righi, Tavecchio & Inoue 2019a), and again the knowledge of distance is a crucial information for modelling the neutrino production and the cosmic neutrino background radiation.

All these arguments explain the major effort for optical spectroscopic studies of BLL candidates. Because of the above-mentioned weakness of the lines, it is compulsory to secure spectra with high and adequate signal-to-noise (S/N) ratios, in order to be able to measure these features of very low equivalent widths (EWs). This requires the use of telescopes of the 8–10 m class.

For 20 yr, we have embarked on a systematic study of BLL objects, lately focusing on *Fermi* detections, using the European Southern Observatory 8-m Very Large Telescope (VLT) and, more recently, the 10-m Gran Telescopio Canarias (GTC). Optical spectra of ∼250 BLL objects have been produced, adopting various selection criteria of the sources (Sbarufatti et al. 2005a, 2006a, 2008, 2009; Landoni et al. 2012, 2013, 2014, 2015, 2018; Paiano et al. 2016, 2017b,c,d, 2018, 2019a; Falomo et al. 2017).

Here, we present optical spectroscopy of 55 objects, which exhibit a hard gamma-ray spectrum in the Third Catalog of Hard *Fermi*-LAT Sources (3FHL; Ajello et al. 2017). From these observations, we are able to characterize the optical spectral properties and determine the redshift in many objects.

In a coordinated paper (Paiano et al., in preparation), we will point out candidates for detection in the TeV range on the basis of the extrapolation to the very high energy (>∼100 GeV) of the *Fermi* spectra accounting for absorption by the EBL. It is expected that ∼20 per cent of the sources with known redshift considered in this work could be detected with the current Cherenkov telescopes, like MAGIC, and 85 per cent with the future Cherenkov Telescope Array.

2 THE SAMPLE

The objects in our sample were extracted from the 3FHL, which contains 1556 objects detected above >10 GeV over 7 yr of *Fermi* operations. We concentrate on 246 TeV candidates,[1] which are sources revealed with significance >3 at energy >50 GeV. They exhibit a hard spectrum, with photon index $\Gamma \lesssim 2.5$ and integrated flux $F(>10\ \mathrm{GeV}) \gtrsim 10^{-11}$ photons cm^{-2} s^{-1}. Of these, 224 sources are classified by the *Fermi* team as BLL objects and blazar candidates of uncertain type (BCUs): 180 and 44 sources, respectively. Extensive search in the literature shows that 153 of these objects lack a measurement of the redshift or the available value is uncertain. Of these, there are 21 BCUs and 70 BLL objects at $\delta > -20$ and thus well observable in the Northern hemisphere.

Here, we report on extensive optical spectroscopy obtained at the GTC for 42 BLL objects and 13 BCUs (see Table 1 for the properties of our sample).

[1]Flagged as 'C' in the 3FHL.

3 OBSERVATIONS AND DATA REDUCTION

Optical spectra were collected using the spectrograph OSIRIS (Cepa et al. 2003) of the 10.4-m GTC at the Roque de Los Muchachos (La Palma). We used the grism R1000B covering the spectral range 4100–7750 Å and a slit width of 1.2 arcsec.

Data reduction was performed using the IRAF software (Tody 1986, 1993) and standard procedures for long-slit spectroscopy, following the same scheme given in Paiano et al. (2017b,c, 2019a). For each source, at least three spectra were obtained and combined together to obtain the final spectrum. Cosmic rays were removed using the L.A.Cosmic algorithm (van Dokkum 2001). The accuracy of the wavelength calibration is ∼0.1 Å over the whole observed spectral range. The relative flux calibration was performed from the observation of a number of spectrophotometric standard stars secured during each night of the programme. Since most of the spectra were obtained during non-photometric nights, we set the absolute calibration from the comparison of the magnitude of the targets, as from the acquisition image in the *g* band, and that of secondary photometric objects in the field as derived from Pan-STARRS (Panoramic Survey Telescope and Rapid Response System) or SDSS images. Finally, all spectra were dereddened applying the extinction law by Cardelli, Clayton & Mathis (1989) and assuming the value of Galactic extinction $E(B-V)$ derived from the NASA/IPAC Infrared Science Archive 6[2] (Schlafly & Finkbeiner 2011). In Fig. 1, we display all our absolute calibrated and dereddened spectra (upper panel) with the normalized form (bottom panel) obtained through the fit of the continuum with a cubic spline. The spectra are also available in our online data base ZBLLAC.[3]

4 METHODS AND RESULTS

For each spectrum, the S/N ratio was measured, and the minimum detectable EW was evaluated following the procedure described in detail in Paiano et al. (2017c).

The optical spectrum is assumed to be the superposition of a non-thermal component described by a power law and the starlight component of the host galaxy. The latter is in almost all cases a giant elliptical galaxy with $M(R) \sim -22.9$ (Sbarufatti, Treves & Falomo 2005b). We performed a spectral decomposition using these two components for all our targets (see some examples in Fig. 2) and details for the individual sources are reported in the corresponding notes. The visibility of the absorption features due to the host galaxy at a given wavelength depends on the ratio of the two components (N/H, nucleus-to-host ratio) and on the minimum detectable EW (Sbarufatti et al. 2006a). Under this assumption, it is possible to set a lower limit to the redshift, when no absorption lines of the host galaxy are detected. We followed the procedure described in appendix A of Paiano et al. (2017b) to evaluate this redshift lower limit.

Our optical spectroscopy shows that all 55 observed targets are BLL objects, including the 13 targets previously classified as BCUs. No objects like flat-spectrum radio quasars (FSRQs) or narrow-line Seyfert I galaxies were found. In Table 2, we report for each target whether the spectrum exhibits emission lines (labelled as E), galactic lines (G), intervening lines (I), or whether it is lineless (L). For each source, we give the redshift, the spectroscopic redshift lower limit in case of intervening line detection, or a lower limit, estimated following the minimum EW method (described above), when the spectrum is featureless. In Table 3, we give the

[2]http://irsa.ipac.caltech.edu/applications/DUST/
[3]http://web.oapd.inaf.it/zbllac/

Table 1. The sample of the 3FHL TeV candidate objects and journal of the GTC observations.

3FGL name	Counterpart	RA (J2000)	Dec. (J2000)	Class	$E(B-V)$	Obs. date	t_{Exp} (s)	Seeing (arcsec)	g
3FHL J0009.4+5030	NVSS J000922+503028	00:09:22.8	50:30:28.8	BLL	0.13	2018 November 6	4500	1.5	18.9
3FHL J0015.7+5551	GB6J0015+5551	00:15:40.1	55:51:45.0	BLL	0.37	2018 November 6	3000	1.5	18.7
3FHL J0045.3+2127	GB6J0045+2127	00:45:19.3	21:27:40.0	BLL	0.03	2018 November 6	1200	1.7	17.7
3FHL J0045.7+1217	GB6J0045+1217	00:45:43.3	12:17:12.0	BLL	0.07	2018 November 26	3000	2.0	17.6
3FHL J0131.1+6120	1RXS J013106.4+612035	01:31:07.3	61:20:34.0	BLL	0.79	2018 December 3	3600	1.3	20.3
3FHL J0134.4+2638	1RXS J013427.2+263846	01:34:28.1	26:38:43.0	BCU	0.09	2017 December 3	1000	1.3	17.6
3FHL J0137.9+5815	1RXS J013748.0+581422	01:37:50.4	58:14:11.0	BLL	0.45	2019 January 3	3600	1.2	18.9
3FGL J0141.4−0929	PKS 0139−09	01:41:25.8	−09:28:43.7	BLL	0.02	2017 December 27	1350	1.1	16.8
3FHL J0148.2+5201	GB6J0148+5202	01:48:20.2	52:02:06.0	BLL	0.19	2018 December 4	2400	2.7	18.1
3FHL J0241.3+6543	TXS0237+655	02:41:21.6	65:43:11.9	BCU	1.09	2016 December 7	3600	0.9	20.9
3FHL J0250.5+1712	NVSS J025037+171209	02:50:37.9	17:12:09.0	BLL	0.12	2018 October 30	1200	1.7	17.8
3FHL J0322.0+2336	MG3J032201+2336	03:22:00.0	23:36:11.0	BLL	0.17	2018 October 30	1200	1.3	17.5
3FHL J0423.8+4149	4C+41.11	04:23:56.0	41:50:02.7	BLL	0.63	2018 March 26	7200	1.9	20.3
3FHL J0433.1+3227	NVSS J043307+322840	04:33:07.7	32:28:40.0	BLL	0.38	2018 November 8	3900	0.7	19.7
3FHL J0433.6+2905	MG2J043337+2905	04:33:37.8	29:05:55.4	BLL	0.66	2017 February 21	4500	1.9	21.9
3FHL J0434.7+0921	TXS0431+092	04:34:41.0	09:23:49.0	BCU	0.22	2017 December 5	3900	1.6	18.1
3FHL J0500.3+5238	GB6J0500+5238	05:00:21.4	52:38:02.0	BCU	0.75	2016 November 26	3600	1.4	19.6
3FHL J0506.0+6113	NVSS J050558+611336	05:05:58.8	61:13:36.0	BLL	0.55	2018 December 14	4800	2.0	19.6
3FHL J0515.8+1528	GB6J0515+1527	05:15:47.3	15:27:17.0	BLL	0.47	2019 March 3	7200	1.7	18.9
3FHL J0540.5+5823	GB6J0540+5823	05:40:30.0	58:23:38.0	BLL	0.34	2018 January 28	900	1.7	18.2
3FHL J0600.3+1245	NVSS J060015+124344	06:00:15.0	12:43:43.0	BCU	0.41	2016 November 28	3600	0.9	18.5
3FHL J0601.0+3837	B20557+38	06:01:02.8	38:38:29.0	BLL	0.46	2019 March 9 and 10	6000	1.6	20.5
3FHL J0602.0+5316	GB6J0601+5315	06:02:00.4	53:16:00.0	BCU	0.15	2017 December 3	900	1.2	17.0
3FHL J0607.4+4739	TXS0603+476	06:07:23.2	47:39:47.0	BLL	0.16	2019 January 20	1200	1.1	17.2
3FHL J0612.8+4122	B30609+413	06:12:51.2	41:22:37.0	BLL	0.17	2019 January 20	900	1.2	18.1
3FHL J0620.6+2645	RXJ0620.6+2644	06:20:40.0	26:43:32.0	BCU	0.34	2019 April 9	3600	1.8	18.5
3FHL J0640.0−1254	TXS0637−128	06:40:07.2	12:53:14.2	BCU	0.49	2017 February 24	1500	1.5	17.9
3FHL J0702.6−1950	TXS0700−197	07:02:42.9	−19:51:22.0	BLL	0.42	2019 March 10	750	1.9	19.1
3FHL J0706.5+3744	GB6J0706+3744	07:06:31.7	37:44:36.0	BLL	0.06	2018 November 2	1800	2.5	17.6
3FHL J0708.9+2240	GB6J0708+2241	07:08:58.3	22:41:36.0	BLL	0.05	2018 December 3	4500	1.2	17.4
3FHL J0709.1−1525	PKS 0706−15	07:09:12.3	−15:27:00.0	BCU	0.55	2018 December 4	7200	2.5	18.9
3FHL J0723.0−0732	1RXS J072259.5−073131	07:22:59.7	−07:31:35.0	BLL	0.21	2018 December 14	3000	1.2	18.1
3FHL J0811.9+0237	PMN J0811+0237	08:12:01.8	02:37:33.0	BLL	0.02	2018 December 4	7200	2.0	18.0
3FHL J0816.4−1311	PMN J0816−1311	08:16:27.2	−13:11:52.0	BLL	0.07	2018 February 22[a]	5400	1.8	17.2
3FHL J0905.5+1357	MG1J090534+1358	09:05:35.0	13:58:06.0	BLL	0.03	2018 February 17[b]	850	1.2–2.0	16.2–17.3[b]
3FHL J0910.5+3329	Ton1015	09:10:37.0	33:29:24.0	BLL	0.02	2018 February 22	350	1.5	16.2
3FHL J0953.0−0840	PMN J0953−0840	09:53:02.7	−08:40:18.0	BLL	0.04	2018 February 22	900	1.5	16.8
3FHL J1037.6+5711	GB6J1037+5711	10:37:44.3	57:11:56.0	BLL	0.01	2018 April 30	1050	1.2	16.5
3FHL J1055.6−0125	NVSS J105534−012617	10:55:34.3	−01:26:16.0	BLL	0.04	2018 December 14	3000	1.3	18.6
3FHL J1059.1−1134	PKS B1056−113	10:59:12.4	−11:34:23.0	BLL	0.02	2019 January 22	900	1.8	17.6
3FHL J1150.5+4154	RBS1040	11:50:34.7	41:54:40.9	BLL	0.02	2019 January 20	900	1.3	17.0
3FHL J1233.7−0145	NVSS J123341−014426	12:33:41.3	−01:44:24.0	BLL	0.03	2019 January 20	3600	1.9	20.3
3FHL J1253.1+5300	S41250+53	12:53:11.9	53:01:12.0	BLL	0.01	2019 January 20	1200	1.2	16.6
3FHL J1418.4−0233	NVSS J141826−023336	14:18:26.3	−02:33:34.0	BLL	0.05	2018 April 30	1050	1.2	16.4
3FHL J1445.0−0326	RBS1424	14:45:06.3	−03:26:12.0	BLL	0.08	2019 April 9	3600	1.2	17.8
3FHL J1447.9+3608	RBS1432	14:48:00.6	36:08:32.0	BLL	0.01	2019 April 16	1500	1.8	16.2
3FHL J1454.5+5124	TXS1452+516	14:54:27.1	51:24:34.0	BLL	0.02	2019 April 10	3600	1.0	16.7
3FHL J1503.7−1541	RBS1457	15:03:40.6	−15:41:14.0	BLL	0.10	2019 April 16	3600	2.0	17.8
3FHL J1549.9−0659	NVSS J154952−065907	15:49:52.0	−06:59:07.0	BCU	0.14	2018 April 9	7200	1.7	18.1
3FHL J1748.6+7006	S41749+70	17:48:32.8	70:05:50.7	BLL	0.03	2018 March 29	1500	0.9	16.6
3FHL J1800.5+7827	S51803+784	18:00:45.7	78:28:04.0	BLL	0.04	2018 August 11	900	2.5	16.7
3FHL J1841.3+2909	MG3J184126+2910	18:41:21.7	29:09:41.0	BCU	0.21	2018 March 31	1200	1.8	18.2
3FHL J1904.1+3627	MG2J190411+3627	19:04:11.9	36:26:59.0	BCU	0.08	2018 April 7	1600	2.0	17.3
3FHL J1911.5−1908	PMN J1911−1908	19:11:29.7	−19:08:23.0	BCU	0.14	2018 May 12	1200	2.0	18.0
3FHL J1921.8−1607	PMN J1921−1607	19:21:51.5	−16:07:13.2	BLL	0.16	2018 October 18[c]	5400	2.5	17.6

Notes. Column 1: *Fermi* name of the target; column 2: counterpart name of the target; columns 3 and 4: right ascension and declination of the optical counterpart; column 5: source classification reported in the 3FHL (BLL = BL Lac object; BCU = blazar candidate of uncertain type); column 6: $E(B-V)$ taken from the NASA/IPAC Infrared Science Archive (https://irsa.ipac.caltech.edu/applications/DUST/); column 7: date of observation; column 8: total integration time; column 9: seeing during the observation; column 10: g magnitude measured from the acquisition image.

[a]This source was observed also on 2018 December 14 and 2019 April 4.

[b]This source was observed also on 2019 March 9 and the source was found in two different flux states.

[c]This source was also discussed in Paiano et al. (2017d).

measurement of all the detected lines and in Fig. 3 we display some close-ups of the normalized spectra around interesting detected features. In 12 objects, we detected emission lines and in 20 we found intrinsic absorption lines. This allows us the determination of 26 new redshifts, ranging from $z = 0.05$ to $z = 0.91$. The mean value is ∼0.28. In five sources, intervening lines are detected, in most cases due to Mg II, which enable to set a robust spectroscopic lower limit to the redshift. These intervening lines originate at redshift in the range between 0.1 and 1.1. The intervening lines are an efficient tool for finding the most distant sources. For the remining 24 sources, we provide the redshift lower limits based on the lack of detection of spectral features. These limits range from $z > 0.1$ to $z > 0.6$.

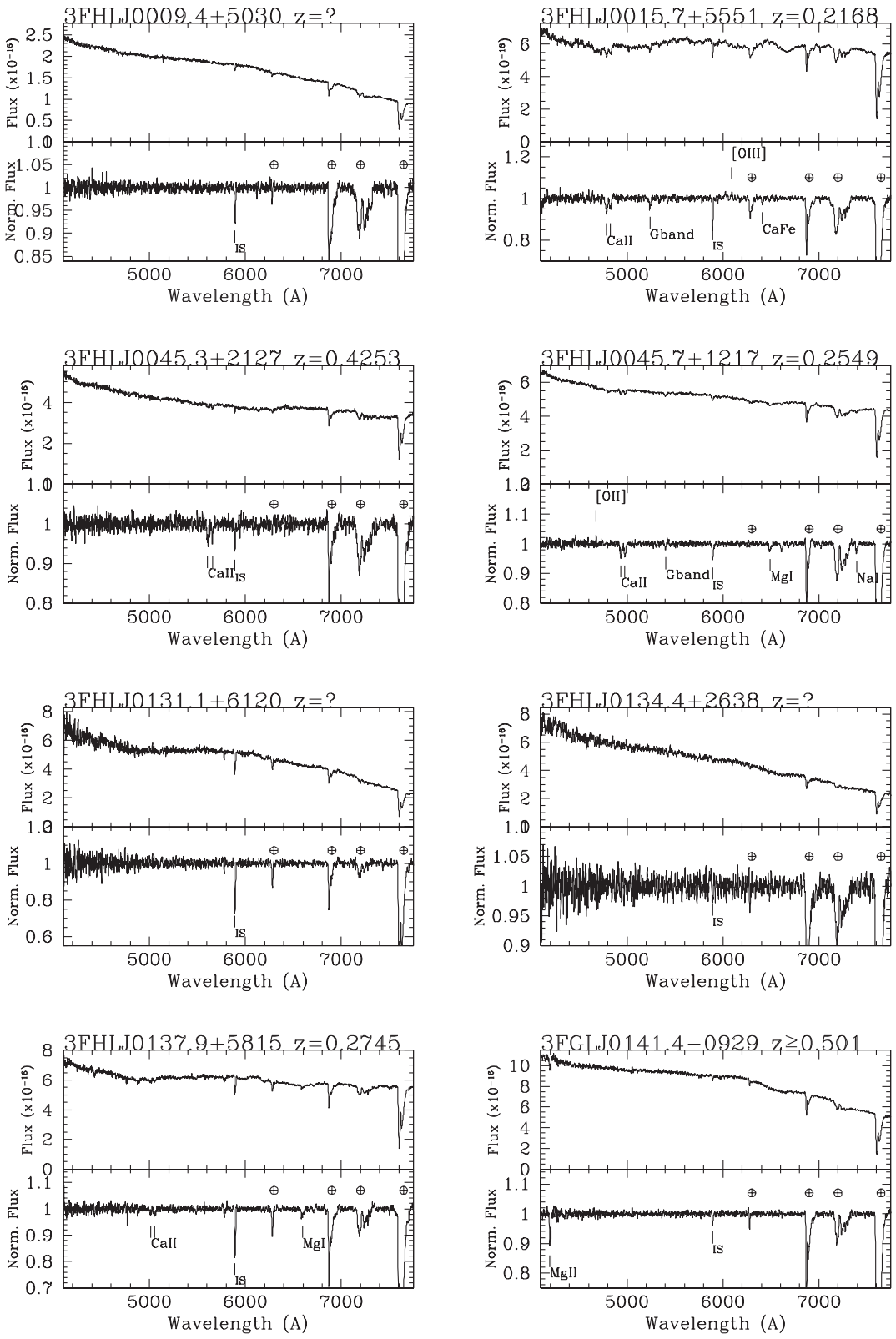

Figure 1. Spectra of the unassociated gamma-ray sources obtained at the GTC. Top panel: Flux-calibrated and dereddened spectra. Bottom panel: Normalized spectra. The main telluric bands are indicated by the circled plus symbols, and the absorption features from interstellar medium of our Galaxy are labelled as IS (interstellar). The full version of the figure is available online.

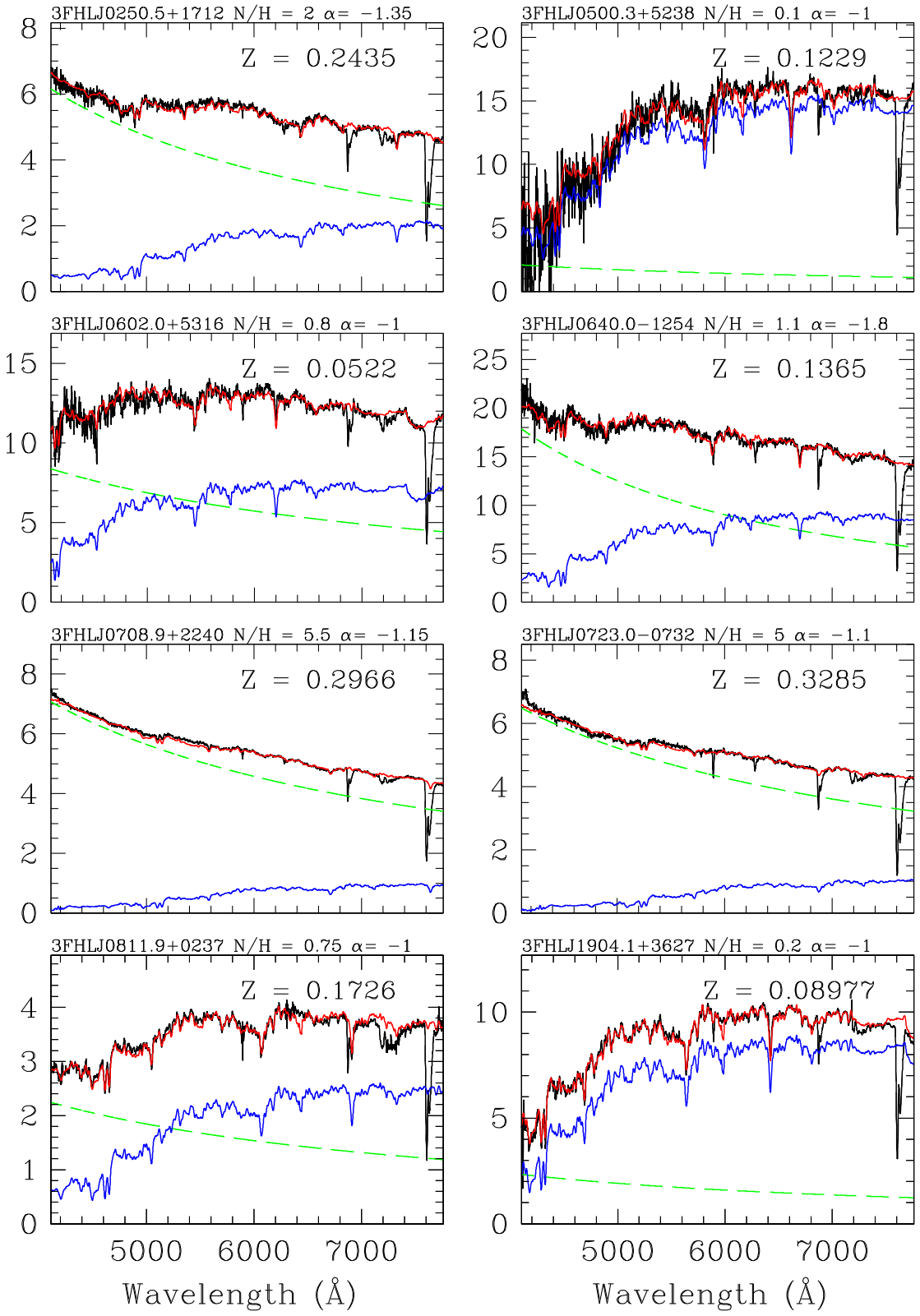

Figure 2. Spectral decomposition of the observed optical spectrum (black line) of selected targets into a power law (green dashed line) and a template of elliptical for the host galaxy (blue line). The fit is given by the red solid line (see text for details). In each panel, the N/H ratio is given together with the spectral index of the power-law component.

Table 2. Properties of the optical spectra of the 3FHL sample.

Object	S/N ratio	EW_{min}	z	Line type
3FHL J0009.4+5030	160	0.17–0.20	(>0.60)	L
3FHL J0015.7+5551	120	0.25–0.40	0.2168	E, G
3FHL J0045.3+2127	90	0.30	0.4253	G
3FHL J0045.7+1217	200	0.20	0.2549	G
3FHL J0131.1+6120	75	0.20–0.70	(>0.10)	L
3FHL J0134.4+2638	80	0.35–0.50	(>0.15)	L
3FHL J0137.9+5815	145	0.25–0.30	0.2745	G
3FGL J0141.4−0929	200	0.20	≥0.501	I
3FHL J0148.2+5201	110	0.30–0.35	0.437	G
3FHL J0241.3+6543	25	1.10–2.70	0.1211	E, G
3FHL J0250.5+1712	100	0.35–0.45	0.2435	G
3FHL J0322.0+2336	160	0.10–0.25	(>0.25)	L
3FHL J0423.8+4149	40	0.35–1.60	0.3977	E
3FHL J0433.1+3227	110	0.25–0.35	(>0.45)	L
3FHL J0433.6+2905	15	1.35–3.80	0.91?	E
3FHL J0434.7+0921	75	0.30–0.90	(>0.1)	L
3FHL J0500.3+5238	40	0.55–4.00	0.1229	E, G
3FHL J0506.0+6113	70	0.30–0.90	0.538?	G
3FHL J0515.8+1528	130	0.20–0.30	(>0.20)	L
3FHL J0540.5+5823	60	0.40–0.90	(>0.10)	L
3FHL J0600.3+1245	50	0.45–1.85	0.0835	E, G
3FHL J0601.0+3837	40	0.50–1.35	0.662?	G
3FHL J0602.0+5316	70	0.35–1.00	0.0522	G
3FHL J0607.4+4739	100	0.15–0.40	(>0.10)	L
3FHL J0612.8+4122	50	0.35–1.10	≥1.107[b]	I
3FHL J0620.6+2645	75	0.40–0.80	0.1329	G
3FHL J0640.0−1254	80	0.35–0.65	0.1365	E, G
3FHL J0702.6−1950	50	0.50–0.95	(>0.10)	L
3FHL J0706.5+3744	100	0.20–0.35	≥0.1042	I
3FHL J0708.9+2240	250	0.15–0.20	0.2966	G
3FHL J0709.1−1525	70	0.35–1.10	0.1420	E, G
3FHL J0723.0−0732	170	0.10–0.25	0.3285	G
3FHL J0811.9+0237	70	0.40–0.85	0.1726	E, G
3FHL J0816.4−1311	300	0.10	(>0.40)	L
3FHL J0905.5+1357	200	0.10–0.20	0.2239[a]	E
3FHL J0910.5+3329	200	0.10–0.20	(>0.15)	L
3FHL J0953.0−0840	220	0.15–0.25	(>0.15)	L
3FHL J1037.6+5711	300	0.10–0.15	(>0.25)	L
3FHL J1055.6−0125	130	0.20–0.40	(>0.55)	L
3FHL J1059.1−1134	50	0.30–1.15	(>0.10)	L
3FHL J1150.5+4154	200	0.15–0.25	(>0.25)	L
3FHL J1233.7−0145	40	0.45–0.95	(>0.10)	L
3FHL J1253.1+5300	250	0.10–0.20	≥0.6638	I
3FHL J1418.4−0233	200	0.15–0.30	(>0.12)	L
3FHL J1445.0−0326	200	0.10–0.20	(>0.45)	L
3FHL J1447.9+3608	250	0.10–0.20	≥0.738	I
3FHL J1454.5+5124	320	0.05–0.10	(>0.40)	L
3FHL J1503.7−1541	50	0.55–1.25	(>0.10)	L
3FHL J1549.9−0659	200	0.15–0.20	0.418	G
3FHL J1748.6+7006	320	0.10–0.20	(>0.3)	L
3FHL J1800.5+7827	130	0.25–0.40	0.683	E
3FHL J1841.3+2909	40	0.55–1.35	(>0.10)	L
3FHL J1904.1+3627	60	0.40–1.50	0.08977	G
3FHL J1911.5−1908	50	0.55–1.20	0.138	E, G
3FHL J1921.8−1607	125	0.20–0.50	(>0.12)	L

Notes. Column 1: name of the target; column 2: median S/N ratio of the spectrum; column 3: range of the minimum EW derived from different regions of the spectrum; column 4: redshift (the value in parentheses are lower limits based on lack of detection of spectral features following the procedure described in the Paiano et al. 2017a); column 5: type of detected line to estimate the redshift: E = emission line; G = galaxy absorption line; I = intervening absorption assuming Mg II 2800 Å identification; L = lower limit derived on the lack of detection of host galaxy absorption lines assuming a BLL elliptical host galaxy with $M(R) = -22.9$ (see details in Paiano et al., 2017b).

[a]The redshift is tentative due to the detection of only one feature.

[b]For this source, we found other two absorption line systems due to Fe II (2382, 2600) (see details in the text).

Table 3. Measurements of the detected lines.

Object name	λ (Å)	EW (Å)	Line ID	Line luminosity (erg s^{-1})
3FHL J0015.7+5551	4787	1.6	Ca II 3934	
	4829	1.0	Ca II 3968	
	5238	1.0	*G*-band 4305	
	6093	−0.5	[O III] 5007	4.2×10^{40}
	6411	0.4	Ca + Fe 5269	
3FHL J0045.3+2127	5607	1.0	Ca II 3934	
	5656	0.5	Ca II 3968	
3FHL J0045.7+1217	4679	−0.2	[O II] 3727	2.3×10^{40}
	4936	1.0	Ca II 3934	
	4980	0.9	Ca II 3968	
	5403	0.3	*G*-band 4305	
	6489	0.6	Mg I 5175	
	6612	0.5	Ca + Fe 5269	
	7393	0.5	Na I 5892	
3FHL J0137.9+5815	5013	0.4	Ca II 3934	
	5057	0.6	Ca II 3968	
	6596	0.9	Mg I 5175	
3FGL J0141.4−0929	4197	1.0	Mg II 2796	
	4207	0.5	Mg II 2803	
3FHL J0148.2+5201	5654	1.3	Ca II 3934	
	5703	1.5	Ca II 3968	
	6183	0.8	*G*-band 4305	
3FHL J0241.3+6543	6607	2.8	Na I 5892	
	7358	−1.7	H α 6563	1.3×10^{41}
	7381	−2.5	[N II] 6584	2.0×10^{41}
	7531	−2.0	[S II] 6716	1.3×10^{41}
	7545	−1.4	[S II] 6731	8.7×10^{40}
3FHL J0250.5+1712	4890	1.7	Ca II 3934	
	4932	1.5	Ca II 3968	
	5090	0.5	H δ 4102	
	5352	0.6	*G*-band 4305	
	6045	0.6	H β 4861	
	6433	0.8	Mg I 5175	
	6549	0.6	Ca + Fe 5269	
	7324	1.9	Na I 5892	
3FHL J0423.8+4149	6998	−1.9	[O III] 5007	5.5×10^{41}
3FHL J0433.6+2905	∼5340	−9.5	Mg II 2800	2.5×10^{42}
3FHL J0500.3+5238	4833	3.5	*G*-band 4305	
	5459	3.1	H β 4861	
	5811	1.6	Mg I 5175	
	5917	2.3	Ca + Fe 5269	
	6617	4.7	Na I 5892	
	7369	−0.3	H α 6563	1.7×10^{40}
	7393	−1.3	[N II] 6584	8.7×10^{40}
3FHL J0506.0+6113	6042	0.8	Ca II 3934	
	6096	0.6	Ca II 3968	
3FHL J0600.3+1245	4664	1.6	*G*-band 4305	
	5267	1.8	H β 4861	
	5608	2.3	Mg I 5175	
	5709	1.6	Ca + Fe 5269	
	6385	3.1	Na I 5892	
	7111	−1.2	H α 6563	2.3×10^{40}
	7133	−1.8	[N II] 6584	3.5×10^{40}
3FHL J0601.0+3837	6538	2.5	Ca II 3934	
	6596	2.0	Ca II 3968	
3FHL J0602.0+5316	4139	2.8	Ca II 3934	
	4176	1.5	Ca II 3968	
	4529	2.1	*G*-band 4305	
	5115	0.6	H β 4861	
	5446	1.3	Mg I 5175	
	5543	0.7	Ca + Fe 5269	
	6200	1.8	Na I 5892	
3FHL J0612.8+4122	5022	1.5	Fe II 2382	
	5450	0.4	Fe II 2586	
	5478	1.5	Fe II 2600	
	5891	3.5	Mg II 2796	
	5906	3.1	Mg II 2803	
3FHL J0620.6+2645	4456	2.8	Ca II 3934	
	4496	3.7	Ca II 3968	
	4876	1.7	*G*-band 4305	
	5507	1.2	H β 4861	
	5863	2.6	Mg I 5175	
	5969	0.8	Ca + Fe 5269	
	6676	2.1	Na I 5892	
	7435	0.4	H α 6563	
3FHL J0640.0−1254	4471	0.4	Ca II 3934	
	4510	0.8	Ca II 3968	
	4892	1.6	*G*-band 4305	
	5525	0.7	H β 4861	
	5882	2.2[a]	Mg I 5175	
	5988	0.7	Ca + Fe 5269	
	6697	1.4	Na I 5892	
	7482	−0.6	[N II] 6584	4.7×10^{40}
3FHL J0706.5+3744	4344	0.4	Ca II 3934	
	4382	0.6	Ca II 3968	
3FHL J0708.9+2240	5100	0.4	Ca II 3934	
	5146	0.5	Ca II 3968	
	5581	0.3	*G*-band 4305	
	6710	0.5	Mg I 5175	
	6832	0.2	Ca + Fe 5269	
3FHL J0709.1−1525	4492	5.3	Ca II 3934	
	4532	4.6	Ca II 3968	
	4916	1.7	*G*-band 4305	
	5552	1.9	H β 4861	
	6017	1.3	Ca + Fe 5269	
	6729	2.3	Na I 5892	
	7518	−1.0	[N II] 6584	3.4×10^{40}
3FHL J0723.0−0732	5226	0.5	Ca II 3934	
	5272	0.9	Ca II 3968	
	5718	0.5	*G*-band 4305	
3FHL J0811.9+0237	4613	4.7	Ca II 3934	
	4653	4.5	Ca II 3968	
	5047	1.6	*G*-band 4305	
	5700	2.7	H β 4861	
	6069	3.0	Mg I 5175	
	6178	1.9	Ca + Fe 5269	
	6910	6.0[a]	Na I 5892	
	7720	−0.3	[N II] 6584	9.8×10^{39}
3FHL J0905.5+1357	6128	−0.7[b]	[O III] 5007	8×10^{40}[b]
3FHL J1253.1+5300	4652	0.3	Mg II 2796	
	4664	0.2	Mg II 2803	
3FHL J1447.9+3608	4859	0.4	Mg II 2796	
	4872	0.2	Mg II 2803	
3FHL J1549.9−0659	5578	1.1	Ca II 3934	
	5627	0.9	Ca II 3968	
	6104	0.5	*G*-band 4305	
3FHL J1800.5+7827	4712	−8.3	Mg II 2800	2.2×10^{43}
3FHL J1904.1+3627	4287	6.0	Ca II 3934	
	4325	5.9	Ca II 3968	
	4691	3.6	*G*-band 4305	
	5298	2.6	H β 4861	
	5640	3.5	Mg I 5175	
	5742	2.1	Ca + Fe 5269	
	6421	3.6	Na I 5892	
3FHL J1911.5−1908	4242	−2.8	[O II] 3727	8.3×10^{40}
	4474	4.1	Ca II 3934	
	4514	2.9	Ca II 3968	
	4896	3.3	*G*-band 4305	
	5529	1.3	H β 4861	
	5695	−0.9	[O III] 5007	2.8×10^{40}
	5886	3.3	Mg I 5175	
	5993	2.2	Ca + Fe 5269	
	6702	3.0	Na I 5892	
	7448	−0.7[c]	[N II] 6548	1.5×10^{40}
	7465	−0.6[c]	H α 6563	1.3×10^{43}
	7489	−2.6	[N II] 6584	6.3×10^{40}

Table 3 – *continued*

Notes. Column 1: name of the target; column 2: barycentre of the detected line; column 3: measured EW; column 4: line identification; column 5: line luminosity.

[a]The line is partially contaminated by a telluric band or the interstellar Na I absorption of our Galaxy.

[b]This is the average EW (EW = 0.5 Å when the source is in high state and EW = 0.9 Å in the low state).

[c]These lines are very faint and blended.

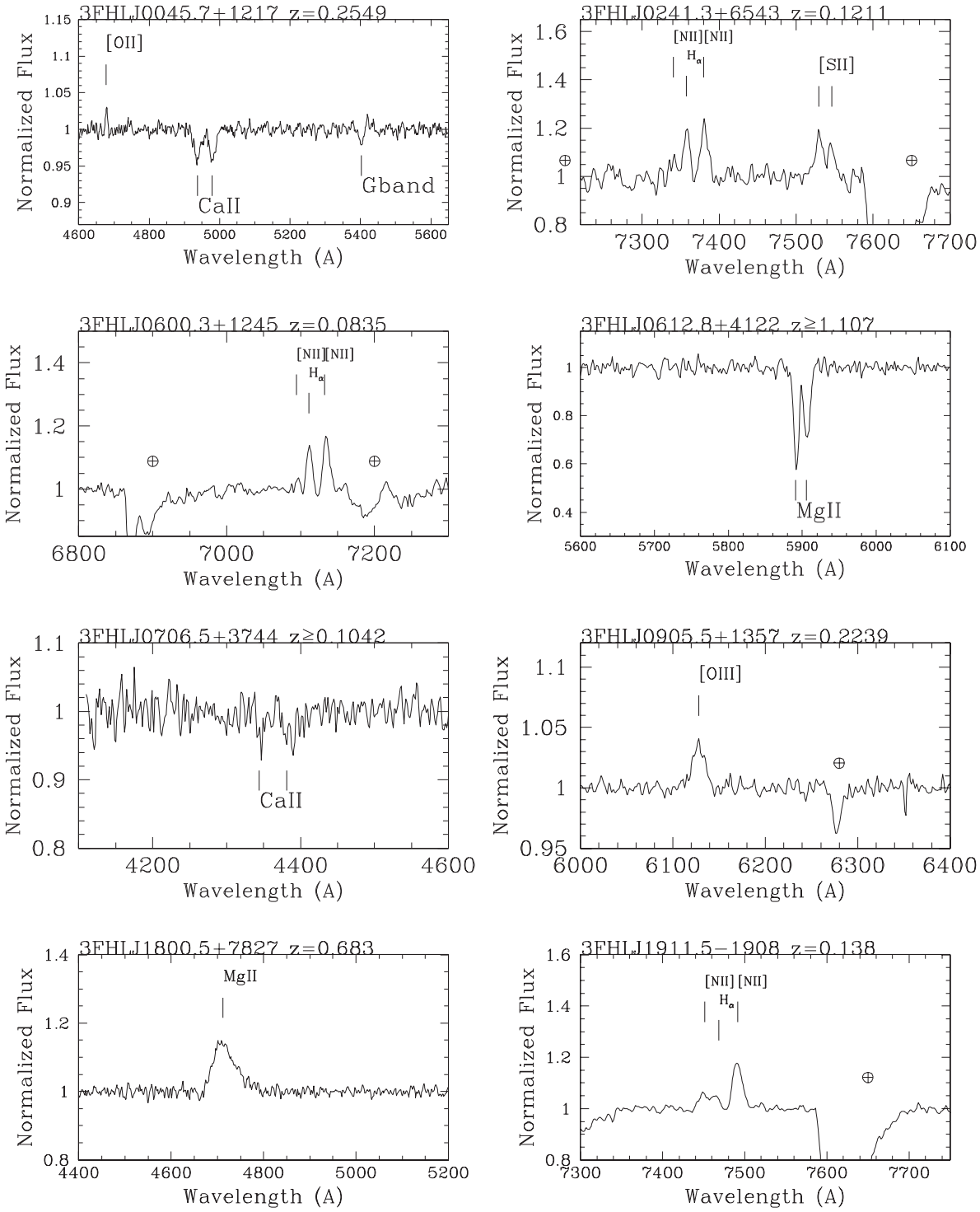

Figure 3. Some examples of close-up of the normalized spectra, obtained at the GTC of the 3FHL TeV candidate objects, around the detected spectral lines. Main telluric bands are indicated as circled plus symbols, and spectral lines are marked by line identification.

5 NOTES ON INDIVIDUAL SOURCES

3FHL J0009.4+5030: The spectrum appears featureless and no emission/absorption lines are detected. On the basis of the minimum EW (∼0.20 Å) and the lack of detection of features from the host galaxy, we can set a redshift lower limit of $z > 0.6$.

3FHL J0015.7+5551: The observed optical counterpart ($g = 18.7$) of this gamma-ray source is at (RA, Dec.) = (00:15:40, +55:51:45) and spatially coincident there is one X-ray source (J001540+555144), detected by *Swift*, and one radio source (NVSS J001540+555144). The dereddened [$E(B - V) = 0.37$] spectrum of the source is characterized by stellar absorption features

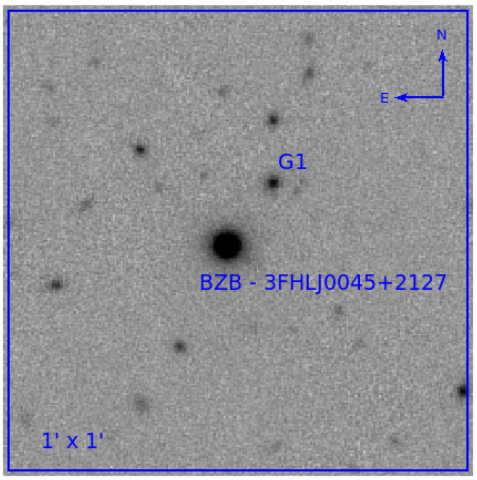

Figure 4. Pan-STARRS *i*-band image of the BLL 3FHL J0045+2127. There is one close companion at ∼10 arcsec from the target (that is at the centre). Field shown is 1 arcmin, North up and East left.

of the host galaxy (Ca II 3934, 3968, *G*-band 4305, Ca + Fe 5269) at $z = 0.2168$, superposed on a non-thermal power-law continuum ($F_\lambda \propto \lambda^\alpha$, $\alpha = -1.2$). From the spectral decomposition of the two components, we set N/H = 1.5. This object was previously studied by Álvarez Crespo et al. (2016), who due to low S/N ratio of the spectrum failed to detect the absorption features. At ∼2.5 arcsec (West on the right), there is a faint companion ($g = 20.7$) that was placed in the slit during our observation and exhibits a stellar spectrum.

3FHL J0045.3+2127: Our optical spectrum (S/N ∼ 90) is characterized by a power-law emission ($\alpha = -1.3$). We detect a faint absorption doublet at ∼5600 Å that we identify as Ca II 3934, 3968 at $z = 0.4253$. It is worth noting that there is a galaxy close to our target at a projected distance of ∼10 arcsec (see Fig. 4) with a redshift of $z = 0.4265$ provided by the Sloan Digital Sky Survey (SDSS). A previous spectrum provided by the SDSS failed to detect any feature, while Shaw et al. (2013) provided a lower limit compatible with our measurement.

3FHL J0045.7+1217: In our spectrum, we find absorption lines due to Ca II 3934, 3968, *G*-band 4305, Mg I 5175, and Ca + Fe 5269 attributed to the stellar population of the host galaxy. In addition, we also detect a faint (EW = 0.2 Å) emission line due to [O II] 3727 (see Fig. 3). The redshift is 0.2549. This is consistent with the lower limit proposed by Shaw et al. (2013). From the spectral decomposition, we set N/H ∼ 4.5 and $\alpha = -1.0$ for the nuclear power-law component.

3FHL J0131.1+6120: The dereddened spectrum [$E(B - V) = 0.79$] is featureless with a minimum detectable EW varying between 0.20 and 0.70 Å along the spectrum. We can set a lower limit of the redshift of $z > 0.10$.

3FHL J0134.4+2638: We obtain an optical spectrum that is featureless. No emission or absorption lines are detected out to a minimum EW of 0.35–0.50 Å. This is consistent with the featureless spectrum of the SDSS. From the lack of detection of host galaxy features, we can set a redshift lower limit of $z > 0.15$. An optical spectrum obtained by Marchesi, Kaur & Ajello (2018) exhibits a prominent emission line at ∼4400 Å, which is interpreted as Mg II 2800. We suspect that the reported line is a spurious artefact. In fact, this feature is not reported in the SDSS spectrum and in Shaw et al. (2013).

3FHL J0137.9+5815: Our spectrum (S/N ∼ 145) is dominated by non-thermal continuum. We detect very weak absorption features from the host galaxy (Ca II 3934, 3968, Mg I 5175, and Ca + Fe 5269), yielding $z = 0.2745$, and from the spectral decomposition we obtain N/H ∼ 3. No previous spectrum is available in the literature.

3FGL J0141.4−0929: The only feature in our spectrum is an absorption doublet at ∼4200 Å, which is due to intervening Mg II 2800, yielding a spectroscopic lower limit of the redshift of $z \geq 0.501$. This feature is also present in the spectra reported in Stickel, Fried & Kuehr (1993) and Stocke and Rector (1997). Note that we do not confirm the emission of Mg II 2800 and [O II] 3727 at $z = 0.737$ proposed by Stocke and Rector (1997).

3FHL J0148.2+5201: In our spectrum, the Ca II 3934, 3968 doublet is apparent at ∼5670 Å and, together with the *G*-band 4305 absorption line at 6183 Å, yields $z = 0.437$. The decomposition of the spectrum provides N/H ∼ 5 and $\alpha = 1.3$ for the nuclear power-law component. The spectrum published by Álvarez Crespo et al. (2016), with a poorer S/N ratio, is featureless.

3FHL J0241.3+6543: We detect two emission lines at ∼7370 Å, which can be interpreted as H α 6563 and [N II] 6584 at $z = 0.1211$ (see the close-up in Fig. 3). At the same redshift, there is a further emission doublet that we attribute to [S II] 6716, 6731, and an absorption line due to Na I 5892. We note that Marchesi et al. (2018), on the basis of an absorption doublet at ∼4600 Å, identified as Mg II, suggest a redshift lower limit of $z \geq 0.645$. This conflicts with our redshift determination.

3FHL J0250.5+1712: We obtain a spectrum with S/N ∼ 100, which exhibits clear absorption lines attributed to the host galaxy (Ca II 3934, 3968, H δ 4861, *G*-band 4305, Mg I 5175, H β 4861, and Na I 5892). This yields a redshift of $z = 0.2435$, confirming the proposal of Archambault et al. (2016). For the emission lines, the upper limit of EW is ∼0.45 Å. The presence of the host galaxy is well detected in the decomposition reported in Fig. 2, where N/H = 2 is estimated.

3FHL J0322.0+2336: Our optical spectrum, with S/N > 160, is largely superior to that reported by Laurent-Muehleisen et al. (1998), but still no significant features are present. The upper limit for the emission/absorption lines is EW = 0.10–0.25 Å, corresponding to a lower limit of the redshift of $z > 0.25$.

3FHL J0423.8+4149: We detect a single emission line at 6997.6 Å with EW = 1.9 Å. The most plausible identification of this line is [O III] 5007 that yields a tentative redshift of $z = 0.3977$. The other component of [O III] 4959 doublet is washed out by the telluric band at 6870 Å. This target was proposed as a neutrino source by Righi, Tavecchio & Pacciani (2019b) and Paiano et al. (2019b).

3FHL J0433.1+3227: Even though our optical spectrum (S/N ∼ 100) is of higher quality than that presented by Álvarez Crespo et al. (2016) (S/N ∼ 5), we still do not find significant features, and from the minimum detectable EW ∼ 0.3 Å, we can set a redshift lower limit of $z > 0.45$.

3FHL J0433.6+2905: The spectrum is severely reddened with $E(B - V) = 0.66$. There is a possible broad emission feature centred at ∼5340 Å in a region of the spectrum where S/N ∼ 15. A similar feature may be present in the spectrum reported in Shaw et al. (2013), but not identified by the authors. Supposing that this feature is due Mg II 2800, the redshift would be ∼0.91.

3FHL J0434.7+0921: In our spectrum, no spectral feature is apparent. We set a lower limit of $z > 0.1$ from the lack of absorption lines from the host galaxy.

3FHL J0500.3+5238: The target is highly reddened with $E(B - V) = 0.75$. Several photospheric absorption lines are apparent (*G*-band 4305, H β 4861, Mg I 5175, Na I 5892, and H α 6564), yielding $z = 0.1229$. At the same redshift, there is a narrow emission line attributed to [N II] 6584 with EW ∼ 1.3 Å. The spectral

decomposition in the power law ($\alpha \sim -1.0$), due to the nucleus, and in the host galaxy template is reported in Fig. 2 and we find N/H = 0.1.

3FHL J0506.0+6113: The optical spectrum (S/N ∼ 70) is highly reddened with $E(B-V) = 0.55$. We find a hint of Ca II 3934, 3968 doublet at 6042, 6096 Å that would correspond to $z \sim 0.54$.

3FHL J0515.8+1528: No significant feature is apparent in our spectrum (S/N ∼ 130). From the null detection of absorption lines of the host galaxy, we can set a lower limit of $z > 0.2$.

3FHL J0540.5+5823: There are no convincing emission/absorption features in our spectrum (S/N ∼ 60). A lower limit of $z > 0.10$ can be set from the lack of detected absorption lines of the host galaxy. This source is inserted in the Padovani et al. (2016) list of hard gamma-ray sources found around the position of IceCube events.

3FHL J0600.3+1245: This gamma-ray object, associated with the radio source NVSS J060015+124344, is classified as BCU in the *Fermi* catalogues. It is spatially coincident with the X-ray source 1RXS J006014.8+124341 and with the optical counterpart at (RA, Dec.) = (06:00:15, 12:43:43). Our optical spectrum exhibits several absorption lines (*G*-band 4305, H β 4861, Mg I 5175, Na I 5892, and H α 6563) attributed to the old stellar population of the host galaxy that allow us to measure $z = 0.0835$. At the same redshift, we also detect, at ∼7133 Å, two narrow emission lines (EW = 1.2 and 1.8 Å) due to H α 6563 and [N II] 6584 (see the close-up in Fig. 3).

3FHL J0601.0+3837: The source was proposed as a BLL object by Paggi et al. (2014) who show a featureless spectrum of the X-ray counterpart. The source is faint ($g = 20.5$) and severely extincted [$E(B-V) = 0.46$], and we obtained a spectrum with S/N ∼ 40. This is basically featureless, apart for a possible doublet (at ∼6560 Å) that, if attributed to Ca II doublet of the host galaxy, corresponds to a redshift of $z = 0.662$.

3FHL J0602.0+5316: The gamma-ray source is associated with the bright radio galaxy GB6J601+5315 and it is inside the error box of a neutrino event detected by IceCube (Padovani et al. 2016). No previous optical spectrum is found in the literature. Our spectrum of the source ($g = 17.0$) shows the absorption lines (Ca II, *G*-band, etc.) of the galaxy stellar population at $z = 0.0522$. The decomposition of the optical spectrum (see Fig. 2) into an elliptical template and a power-law ($\alpha \sim -1.0$) emission indicates the presence of a *non-thermal* component contributing for ∼45 per cent.

3FHL J0607.4+4739: An optical spectrum, obtained by Shaw et al. (2013), does not show any significant features. From our lineless spectrum (S/N = 100), on the basis of the lack of detectable galaxy absorption lines, we can set a redshift lower limit of $z > 0.10$.

3FHL J0612.8+4122: Our spectrum is dominated by a power-law continuum without significant intrinsic emission/absorption lines. However, we clearly detect intervening absorption systems of Mg II 2800, Fe II 2382, and Fe II 2586, 2600 at $z = 1.107$. The Mg II absorption line doublet is also apparent in Shaw et al. (2013).

3FHL J0620.6+2645: This gamma-ray source ($g = 18.5$) is classified as BCU in the *Fermi* catalogues. No previous optical spectrum is available. In our spectrum, many absorption lines from the host galaxy are clearly detected, yielding $z = 0.1329$. The decomposition of the spectrum into an elliptical galaxy and a power-law ($\alpha = -1.5$) emission allows us to set N/H ∼ 0.5.

3FHL J0640.0−1254: No previous redshift is reported in the literature. Our spectrum exhibits absorption lines (Ca II, *G*-band, Mg I, and Na I) of the host galaxy diluted by the non-thermal emission from the nucleus, allowing to measure $z = 0.1365$. The spectral decomposition into the elliptical galaxy and nucleus power-law component provides N/H ∼ 1 (see Fig. 2). In addition to the absorption feature, we also detect a narrow emission line at 7482 Å (EW = 0.6 Å) corresponding to [N II] 6584. We note that the object visible at 6.5 arcsec from the target is a star and it is derived by the GTC spectrum obtained during the same observation of our target.

3FHL J0702.6−1950: No optical spectra are found in the literature. We obtain the spectrum orientating the slit to intersect the target ($g = 19.1$) and the close object at ∼5 arcsec, which is a star (the classification is provided by GTC spectroscopy). The moderate S/N ∼ 50 spectrum of the gamma-ray target is dominated by a featureless continuum characterized by a typical power-law shape with spectral index $\alpha = -1.4$. Based on the lack of spectral features from the host galaxy, we set a lower limit of $z > 0.10$.

3FHL J0706.5+3744: We detect a faint absorption doublet at ∼4350 Å (EW ∼ 0.6 Å) that is attributed to Ca II 3934, 3968 (see Fig. 3), yielding a redshift of $z = 0.1042$. If these lines were ascribed to the starlight of the host elliptical galaxy, we would expect to observe the trace of the host galaxy in the continuum, which is not present. Moreover, these detected lines are narrower, compared to the typical Ca II line width from elliptical galaxies, rather indicating an interstellar absorption origin. Indeed at ∼12 arcsec from the target, there is another galaxy for which we obtained an optical spectrum: we found several emission lines due to H β 4861, [O III] 4959, 5007, and H α 6563 at $z = 0.1042$, the same value of the BLL object. We suppose that the halo gas of this close galaxy (located at the projected distance of ∼23 kpc at that redshift) can be responsible for the absorption doublet found in the spectrum of gamma-ray source. Therefore, for 3FHL J0706.5+3744, we set the spectroscopic lower limit of the redshift of $z \geq 0.1042$.

3FHL J0708.9+2240: This object is a BCU gamma-ray emitter associated with the radio source GB6J0708+2241. The optical counterpart ($g = 17.4$) is at (RA, Dec.) = (07:08:58.3, 22:41:36.0). Massaro et al. (2015) report an optical spectrum without evident features. We detect absorption lines (Ca II, *G*-band, and Mg I) due to the old stellar population of the host galaxy, allowing us to locate the source at $z = 0.2966$. The spectral decomposition, reported in Fig. 2, indicates the presence of a non-thermal power-law component ($\alpha = -1.15$) and N/H = 5.5.

3FHL J0709.1−1525: In the *Fermi* catalogue, this BCU gamma-ray source is associated with the radio source PKS 0706−15. From the analysis of *Swift*/XRT data, inside the Fermi error box we detect the X-ray source J070912−152703, spatially coincident with the radio counterpart and the optical counterpart ($g = 18.9$) at (RA, Dec.) = (07:09:12.3, −15:27:00.0). This confirms the association with PKS 0706−15. No previous spectrum is reported in the literature. Our spectrum, highly reddened [$E(B-V) = 0.55$], exhibits the shape of an elliptical galaxy with evident absorption lines (Ca II, *G*-band, H β, Ca + Fe, Na I, and H α) at a redshift of $z = 0.1420$. In addition, we detect an emission line (EW = 1.0 Å) at 7518 Å, which is attributed to [N II] 6584 Å.

3FHL J0723.0−0732: The blazar classification of this gamma-ray emitter is proposed by Martí et al. (2004) who report a featureless optical spectrum. In our spectrum (S/N ∼ 170), we detect the absorption doublet attributed to Ca II 3934, 3968 and a faint feature due to *G* band. This yields a redshift of $z = 0.3285$. The decomposition of the spectrum (see Fig. 2) into an elliptical template and a power-law emission indicates the presence of a non-thermal component and allows us to set N/H ∼ 5.

3FHL J0811.9+0237: There are not previous spectra available for this object. Our spectrum clearly exhibits absorption lines (Ca II, *G*-band, H β, Mg I, Ca + Fe, and Na I) due to the host elliptical galaxy at $z = 0.1726$. In addition, a faint emission line attributed

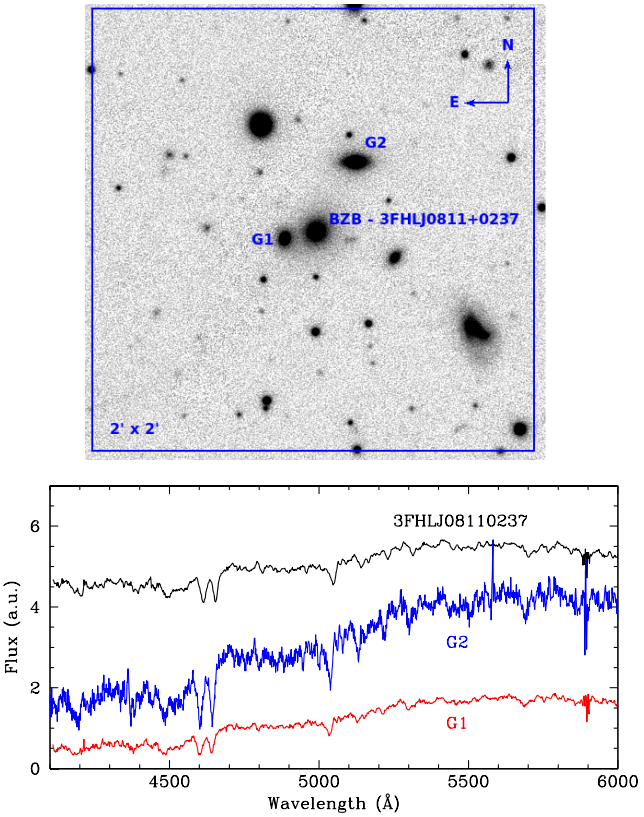

Figure 5. Upper panel: The Pan-STARRS *i*-band image (North up and East left) of the BLL 3FHL J0811.9+0237 (in the centre). There are two close companions of the BLL object: G1 at ∼9 arcsec and G2 at ∼22 arcsec. Bottom panel: Comparison of the BLL spectrum with the spectra of the two companions (see details in the text).

to [N II] 6584 is detected at the same redshift. The decomposition of the spectrum into an elliptical galaxy and a power-law ($\alpha = -1$) emission reveals the presence of a non-thermal component and N/H ∼ 0.75 (see Fig. 2). We note that 3FHL J0811.9+0237 could belong to a small group of galaxies. There are two neighbour galaxies at ∼9 arcsec (on East) and ∼22 arcsec (North-West) at redshift similar to our target (see Fig. 5): from our GTC spectroscopy of G1 and from the SDSS spectrum available for G2, we find that these companions are elliptical galaxies at $z = 0.1697$ of projected velocity of ∼900 km s^{-1} relative to our target.

3FHL J0816.4−1311: Despite the high-quality optical spectrum (S/N ∼ 300), no emission/absorption lines are found. On the basis of the minimum detectable EW (∼0.10 Å) and the lack of feature detection from the host galaxy, we can set a redshift lower limit of $z > 0.40$. There are previous spectra reported in the literature by Shaw et al. (2013), who show a featureless spectrum, and by Pita et al. (2014) who found intervening absorption systems attributed to Mg II 2800 (at $z = 0.1902$, 0.2336, and 0.2882) in a spectral range not covered by our spectrum.

3FHL J0905.5+1357: We observed this source at two different epochs separated by an interval of about 1 yr (see Table 1). It is noticeable that the source magnitude obtained from the acquisition images varied by ∼1 mag. In Fig. 1, we report the average spectrum of the two epochs. The shape is the typical BLL continuum and the only intrinsic feature detected is an emission line (average EW ∼ 0.7 Å) at 6133 Å (see the close-up around this line in Fig. 3), which, if attributed to [O III] 5007, yields a redshift of 0.2239. The line luminosity is ∼8×10^{40} erg s^{-1} during the two states, while the continuum varies by a factor of ∼3. This source is quoted in Padovani et al. (2016) as spatially coincident with the error box of a neutrino IceCube event and there are two previous spectra by Shaw et al. (2013) and the SDSS. Both spectra appear featureless and correspond to a high state of the source [F(6100 Å) ∼ 1×10^{-16} erg cm^{-2} s^{-1}] that probably has hampered the detection of the line, which appeared clearly in our observations when the source was in a lower flux state.

3FHL J0910.5+3329: Our optical spectrum with S/N ∼ 200 appears featureless, in agreement with the previous spectra available in the literature (Bauer et al. 2000; Shaw et al. 2013; and that provided by the SDSS). We can set a redshift lower limit of $z > 0.15$ on the basis of the non-detection of features due to the host galaxy.

3FHL J0953.0−0840: The only spectrum available in the literature is provided by Shaw et al. (2013), which is featureless. In our good optical spectrum (S/N ∼ 220), still no emission/absorption line is detected. The spectrum exhibits the power-law shape, typical for BLL objects, with a spectral index of $\alpha = -1.5$. By the minimum EW method, we can set the redshift lower limit of $z > 0.15$.

3FHL J1037.6+5711: All previous spectra reported in the literature (Laurent-Muehleisen et al. 1998; Caccianiga et al. 2002; Shaw et al. 2013; and the SDSS) do not exhibit emission/absorption lines. Our high-quality (S/N ∼ 300) spectrum shows the typical BLL power-law shape and it still is featureless. The estimated minimum EW is ∼0.15 Å and this yields a redshift lower limit of $z > 0.25$.

3FHL J1055.6−0125: No redshift is reported in the literature. The spectral shape of our spectrum is well described by a power-law emission ($\alpha \sim -1.5$), typical of a BLL object. No emission or absorption features are apparent at the level of EW ∼ 0.40 Å and we can set a redshift lower limit of $z > 0.55$.

3FHL JJ1059.1−1134: The source was observed by Landoni et al. (2013) and Shaw et al. (2013) and they did not detect any features. Also, our spectrum appears featureless. The minimum detectable EW spans between 0.30 and 1.15 Å along the spectrum, allowing us to set a redshift lower limit based on the lack of galaxy absorption lines of $z > 0.10$.

3FHL J1150.5+4154: There is an SDSS spectrum of the source and one in the collection of Shaw et al. (2013). Neither absorption nor emission features are apparent. Also, our high-S/N (∼200) spectrum is featureless, and from the minimum EW ∼ 0.25 Å, we can set a lower limit of $z > 0.25$ from the lack of detection of features from the host galaxy.

3FHL J1233.7−0145: Optical spectra provided by Shaw et al. (2013), Kügler et al. (2014), and from the SDSS are featureless and no spectroscopic redshift is provided. Also, in our spectrum no emission/absorption features are detected, and from a minimum detectable EW ∼ 0.45–0.95 Å, we can set a redshift lower limit of $z > 0.10$.

3FHL J1253.1+5300: In our high-quality spectrum (S/N ∼ 250) of the target ($g = 16.6$), we detect a faint absorption doublet system (EW ∼ 0.3 Å) at ∼4660 Å attributed to intervening Mg II Å cold gas, allowing us to set the spectroscopic redshift lower limit of $z \geq 0.6638$. The same line system is found in the spectrum of the SDSS and reported by Shaw et al. (2013).

3FHL J1418.4−0233: All optical spectra reported in the literature (Shaw et al. 2013; Kügler et al. 2014; and that provided by the SDSS) appear featureless and no redshift is measurable. Our S/N ∼ 200 optical spectrum of this bright target ($g = 16.4$) does not exhibit emission or absorption lines and the minimum detectable EW is ∼0.15–0.30 Å. We can set a redshift lower limit of $z > 0.12$.

3FHL J1445.0−0326: This object has been classified as BLL by Bauer et al. (2000), but its redshift was not determined because of the absence of emission and absorption features. Featureless spectra are reported in Sbarufatti et al. (2006a) and Piranomonte et al. (2007) Also, our spectrum (S/N = 200) does not show apparent spectral lines at the level of EW ∼ 0.20 Å and we can set a redshift lower limit of $z > 0.45$.

3FHL J1447.9+3608: In our spectrum (S/N ∼ 250), there is a clear absorption doublet at 4865 Å, which is due to intervening Mg II 2800 system, yielding a spectroscopic lower limit of $z \geq 0.738$. The feature was noted by Shaw et al. (2013) and appears also in the SDSS spectrum.

3FHL J1454.5+5124: The redshift $z = 1.0831$ reported in the literature was proposed by the automatic procedure of the SDSS. However, no convincing line identification is provided and also the spectrum shown by Shaw et al. (2013) appears featureless. In our spectrum of very good quality, with S/N ∼ 320, no spectral features are found. We can set a redshift lower limit of $z > 0.40$ by the minimum EW ∼ 0.10 Å.

3FHL J1503.7−1541: The optical spectra reported in the literature (Bauer et al. 2000; Sbarufatti et al. 2006a; Shaw et al. 2013) are featureless. Also, our spectrum does not present emission/absorption lines and we can set a redshift lower limit of $z > 0.10$.

3FHL J1549.9−0659: This gamma-ray emitter is associated with the radio source NVSS J154952−065907 and proposed as a blazar candidate in the *Fermi* catalogue because no spectra are available in the literature. Our spectrum establishes the BLL nature of the source and we find faint absorption lines due to Ca II 3934, 3968 and *G*-band 4305, attributed to the stellar population of the host galaxy, at $z = 0.418$.

3FHL J1748.6+7005: In the literature, Stickel, Fried & Kuehr (1989) provided a tentative redshift of $z = 0.77$ based on the identification of the very faint (EW = 0.4 Å) [O II] emission line at 6600 Å. This value was subsequently confirmed by Lawrence et al. (1996) from the detection of additional lines due to C III] (EW = 0.4 Å) and [O III] (EW = 0.7 Å). Our high-S/N (∼300) spectrum of the bright target ($g = 16.6$) is featureless. Note that we cannot detect the emission lines claimed in the previous works because they are out of our spectral range.

3FHL J1800.5+7827: We clearly detect a significant (EW = 8.3 Å) emission line at 4712 Å (see the close-up in Fig. 3) that, if attributed to Mg II 2800, leads to a redshift of $z = 0.683$. From the literature, a similar value is reported in Hewitt and Burbidge (1993) and in Stickel, Meisenheimer & Kuehr (1994) where neither spectrum nor line identification is shown.

3FHL J1841.3+2909: This 3FHL source is associated with the radio source MG3 J184126+2910 and proposed as a BLL candidate (Massaro et al. 2013). Our dereddened [$E(B - V) = 0.21$] optical spectrum is described as a power law ($\alpha = -1.1$) and no evident lines are found. We set a redshift lower limit of $z > 0.1$. There is also another spectrum published by Marchesi et al. (2018) that is again featureless.

3FHL J1904.1+3627: This target is a candidate blazar in the *Fermi* catalogue and associated with the radio source MG2 J190411+3627. In Marchesi et al. (2018), the optical spectrum seems featureless, mainly due to a poor S/N ratio. Our spectrum (S/N ∼ 60) is modelled by an elliptical galaxy shape and shows several absorption lines due to the old stellar population of the host galaxy. The redshift of the target is $z = 0.08977$. From the spectral decomposition (see Fig. 2), we can determine that the AGN contributes to ∼15 per cent (N/H = 0.2).

3FHL J1911.5−1908: This source is a BCU of the *Fermi* catalogue associated with the radio source PMN J1911−1908. Marchesi et al. (2018) report an optical spectrum of modest S/N ratio that appears featureless. In our spectrum, several absorption lines are found due to the old stellar population (Ca II, *G*-band, Mg I, Ca + Fe, and Na I), yielding a redshift of $z = 0.138$. At the same redshift, we also detect narrow emission lines due to forbidden transitions attributed to [O II] 3727, [O III] 5007, [N II] 6548, H α 6563 partially blended, and [N II] 6584.

3FHL J1921.8−1607: Our good (S/N ∼ 125) optical spectrum does not exhibit emission or absorption lines. From the lack of detection of features of the host galaxy, with the minimum detectable EW ∼ 0.20–0.50 Å and magnitude $g = 17.6$, we can set a lower limit of the redshift of $z > 0.12$. In the literature, there is another spectrum in Shaw et al. (2013) that is featureless.

6 SUMMARY AND CONCLUSIONS

From our optical spectroscopy, we can assess that all sources in the observed data set are BLL. We determined the redshift for 26 objects from absorption lines of their host galaxies and in some cases also from emission lines. For other five objects, we found a spectroscopic lower limit from the detection of intervening absorptions. The remaining 24 sources have featureless optical spectra; thus, we estimate a redshift lower limit from the absence of absorption features of the host galaxy. Moreover, for all the latter sources there are not intervening absorptions, which suggests they are at relatively low redshift. Considering the absorptions from Mg II, we expect that the number of Mg II absorbers per redshift bin (dN/dz), with EW > 0.3 Å, is ∼0.5 (Zhu & Ménard 2013). Since none are detected above 4100 Å, one must have on average $\bar{z} < 0.6$. This is consistent with the median value of the detected redshifts ($\bar{z} \sim 0.3$.).

BLL objects are characterized by the lack of (or very weak) features in their optical spectra. Apart from the absorption lines from the host galaxies that are always present if sufficient high-quality spectrum is available (Landoni et al. 2014), it is of interest to evaluate the properties of the possible emission lines compared with other active nuclei. Weak narrow emission lines are observed in a number of cases for BLL objects. These can arise either from a region of significant star formation or from nuclear emission in the narrow-line region (Bressan et al. 2006; Paiano et al. 2017b, 2018). The detection of weak broad emission lines is rarer (see e.g. Sbarufatti et al. 2006b; Landoni et al. 2012). It adds an important ingredient for the understanding of this class of AGNs (e.g. Giommi, Padovani & Polenta 2013), in particular in connection with the FSRQs and the possibility of an evolutionary relation between these two classes (e.g. Giommi et al. 2013; Ajello et al. 2014).

In four objects, we detected weak (EW ∼ 0.5–1.9 Å) [O III] 5007 emission lines (see Table 3). This yields an average line luminosity $L \approx 8 \times 10^{40}$ erg s^{-1}. For the 13 objects of known redshift and for which [O III] would be observable in our spectra, on average we set an upper limit line luminosity of 3×10^{40} erg s^{-1}. A similar limit was also derived for the 24 sources of unknown redshift, assuming that the [O III] emission line be inside the observed range. In addition to the [O III] emission line, we also detect [N II] 6584 emission feature in seven targets (only in one of these cases also [O III] is present). The derived [N II] line luminosity is in the range 0.1–2 $\times 10^{41}$ erg s^{-1}. Only for two sources we detected measurable H α emission. These weak (EW ∼ 1.5 Å) lines imply H α luminosity of 2.5 $\times 10^{40}$ and 1.2 $\times 10^{41}$ erg s^{-1}. At face value, the [O III] line luminosity is

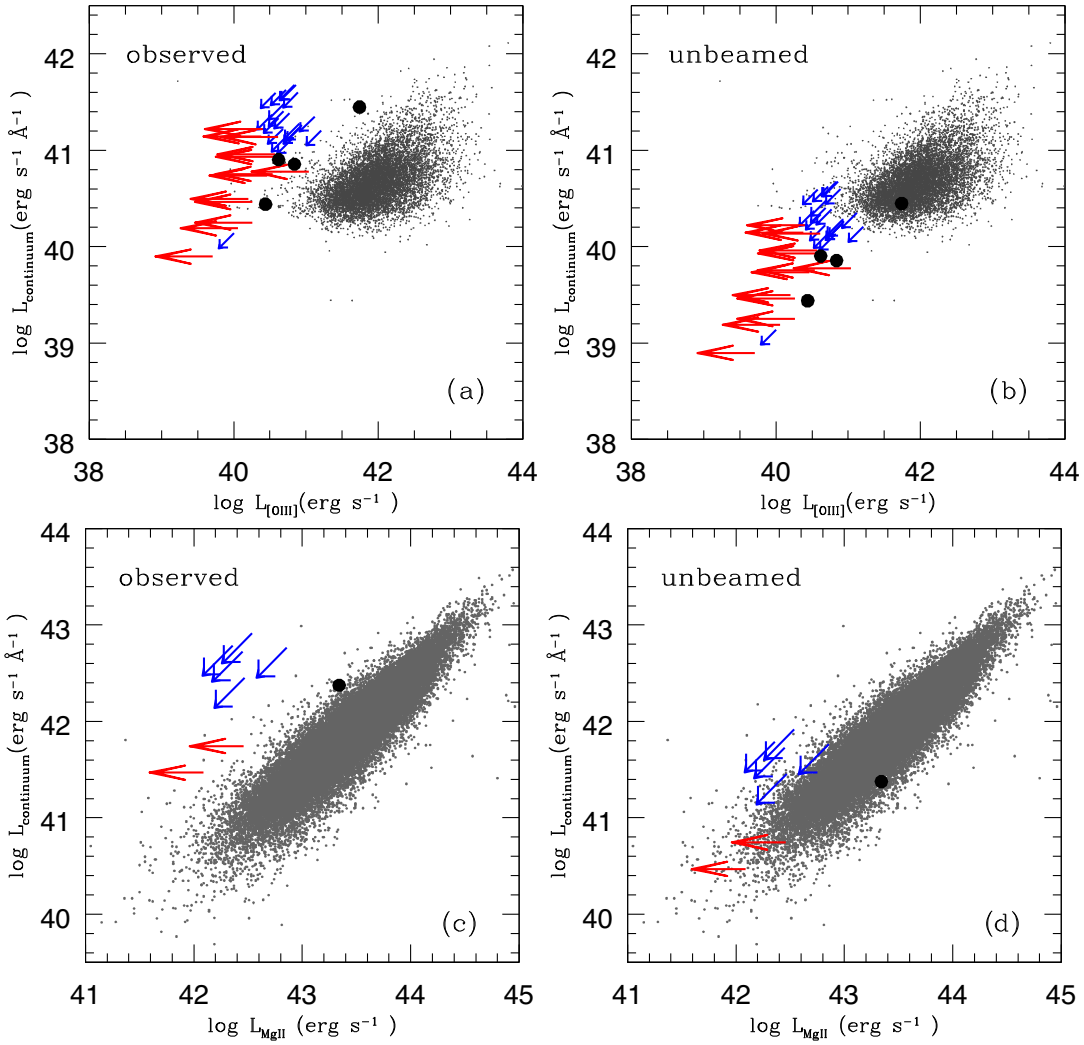

Figure 6. Upper panels: The relation between the [O III] line luminosity and the beamed (a) and unbeamed of a factor 10 (b) continuum luminosity of our sample of 3FHL BLL compared to that of low-redshift ($0.1 < z < 0.5$) QSOs from the SDSS (grey points) taken from Shen et al. (2011). The four cases with detected [O III] emission line are marked with black circles (see also Table 3). The 13 BLL objects with known redshift but without the [O III] line detection are indicated as red arrows and represent upper limits for $L_{[O\ III]}$. Finally, the blue arrows are the upper limits for [O III] and continuum luminosity for the BLL without redshift (see text for details). Bottom panels: The relation between the Mg II line luminosity and the beamed (c) and unbeamed of a factor 10 (d) continuum luminosity of our BLL sample compared to that of QSO (grey points) with redshift $0.46 < z < 1.5$ from Shen et al. (2011). The only case with Mg II line detected is marked with black circle, the two sources with $z > 0.5$ and without Mg II line detection are marked as red arrows, while the BLL objects with spectroscopic redshift lower limit are labelled with blue arrows.

significantly lower than that found for the low-redshift ($0.1 < z < 0.5$) QSOs (see e.g. Shen et al. 2011) at comparable observed continuum luminosity (see Fig. 6a). On average, the [O III] luminosity for our BLL sample is a factor of ∼50 lower than that found for the QSOs ($\sim 10^{42}$ erg s^{-1}) and a factor of ∼20 lower considering the [O III] luminosity distribution of the type II QSOs (see Zakamska et al. 2003). This might indicate either that the lines are indeed fainter than those found in the QSOs at the same continuum level or that the continuum is significantly enhanced by the presence of relativistic beaming that is characteristic of this kind of sources (e.g. Urry & Padovani 1995). Actually, assuming a beaming factor of ∼10, both measured values and upper limits move to the region at the lowest line and continuum luminosities, as displayed in Fig. 6b.

Another important result of our spectroscopy is that we do not find broad emission lines, except for 3FHL J1800.5+7827 for which we detect Mg II emission line of EW = 8.3Å, full width at half-maximum ∼3500 km s^{-1}, and $L_{Mg\,II} = 2.2 \times 10^{43}$ erg s^{-1}. This is at the limit of the distribution of the QSOs at similar redshift and luminosity of the continuum (see Fig. 6c). Among our BLL objects with known redshift, only two are at $z > 0.5$ and the Mg II emission could occur in the observed spectral range. For these sources, we estimate an upper limit of the Mg II luminosity $\leq 2 \times 10^{42}$ erg s^{-1}, which is a factor of 20 smaller than the average value of the QSOs reported in Shen et al. (2011). A similar value is also found for the BLL for which we provide a spectroscopic redshift lower limit. As for the case of [O III] lines, when accounting for the same beaming correction data points and limits are located in the region of the lowest luminosity (see Fig. 6d).

The comparison and contrast of the properties of the emission lines of BLL objects and AGNs obviously require a thorough and extended discussion, which deserve the comparison of large and homogeneous samples to properly investigate this issue.

ACKNOWLEDGEMENTS

The financial contribution by the contract 'Scienza ed osservazioni con LBT' (DD 163/2019 - Ob. Fun. 1.05.03.01.09) of the INAF project 'Supporto Arizona & Italia', is acknowledged.

DATA AVAILABILITY

The flux-calibrated and dereddened spectra are available in our online data base ZBLLAC.[4]

REFERENCES

Abdollahi S. et al., 2020, ApJS, 247, 33
Ahlers M., Halzen F., 2015, Rep. Prog. Phys., 78, 126901
Ajello M. et al., 2014, ApJ, 780, 73
Ajello M. et al., 2017, ApJS, 232, 18
Álvarez Crespo N. et al., 2016, AJ, 151, 32
Archambault S. et al., 2016, AJ, 151, 142
Bauer F. E., Condon J. J., Thuan T. X., Broderick J. J., 2000, ApJS, 129, 547
Bressan A., Falomo R., Valdés J. R., Rampazzo R., 2006, ApJ, 645, L101
Caccianiga A., Marchã M. J., Antón S., Mack K.-H., Neeser M. J., 2002, MNRAS, 329, 877
Cardelli J. A., Clayton G. C., Mathis J. S., 1989, ApJ, 345, 245
Cepa J. et al., 2003, in Iye M., Moorwood A. F. M., eds, Proc. SPIE Conf. Ser. Vol. 4841, Instrument Design and Performance for Optical/Infrared Ground-Based Telescopes. SPIE, Bellingham, p. 1739
Cusumano G. et al., 2010, A&A, 524, A64
D'Abrusco R., Massaro F., Paggi A., Smith H. A., Masetti N., Landoni M., Tosti G., 2014, ApJS, 215, 14
D'Abrusco R. et al., 2019, ApJS, 242, 4
Falomo R., Scarpa R., Treves A., Urry C. M., 2000, ApJ, 542, 731
Falomo R., Pian E., Treves A., 2014, A&AR, 22, 73
Falomo R., Treves A., Scarpa R., Paiano S., Landoni M., 2017, MNRAS, 470, 2814
Fermi-LAT Collaboration, 2019, preprint (arXiv:1905.10771)
Franceschini A., Rodighiero G., 2017, A&A, 603, A34
Ghisellini G., Tavecchio F., 2009, MNRAS, 397, 985
Ghisellini G., Righi C., Costamante L., Tavecchio F., 2017, MNRAS, 469, 255
Giommi P., Perri M., Piranomonte S., Padovani P., 2002, in Giommi P., Massaro E., Palumbo G., eds, Blazar Astrophysics with BeppoSAX and Other Observatories. ESA-ESRIN, Frascati, Italy, p. 123
Giommi P., Padovani P., Polenta G., 2013, MNRAS, 431, 1914
Hewitt A., Burbidge G., 1993, ApJS, 87, 451
Kügler S. D., Nilsson K., Heidt J., Esser J., Schultz T., 2014, A&A, 569, A95
Landi R., Bassani L., Stephen J. B., Masetti N., Malizia A., Ubertini P., 2015, A&A, 581, A57
Landoni M., Falomo R., Treves A., Sbarufatti B., Decarli R., Tavecchio F., Kotilainen J., 2012, A&A, 543, A116
Landoni M., Falomo R., Treves A., Sbarufatti B., Barattini M., Decarli R., Kotilainen J., 2013, AJ, 145, 114
Landoni M., Falomo R., Treves A., Sbarufatti B., 2014, A&A, 570, A126
Landoni M., Falomo R., Treves A., Scarpa R., Reverte Payá D., 2015, AJ, 150, 181
Landoni M., Paiano S., Falomo R., Scarpa R., Treves A., 2018, ApJ, 861, 130
Laurent-Muehleisen S. A., Kollgaard R. I., Ciardullo R., Feigelson E. D., Brinkmann W., Siebert J., 1998, ApJS, 118, 127
Laurent-Muehleisen S. A., Kollgaard R. I., Feigelson E. D., Brinkmann W., Siebert J., 1999, ApJ, 525, 127
Lawrence C. R., Zucker J. R., Readhead A. C. S., Unwin S. C., Pearson T. J., Xu W., 1996, ApJS, 107, 541
Madejski G., Sikora M., 2016, ARA&A, 54, 725
Maraschi L., Ghisellini G., Celotti A., 1992, ApJ, 397, L5
Marchã M. J. M., Caccianiga A., 2013, MNRAS, 430, 2464
Marchesi S., Kaur A., Ajello M., 2018, AJ, 156, 212
Martí J., Paredes J. M., Bloom J. S., Casares J., Ribó M., Falco E. E., 2004, A&A, 413, 309
Massaro F., Paggi A., Errando M., D'Abrusco R., Masetti N., Tosti G., Funk S., 2013, ApJS, 207, 16
Massaro F. et al., 2015, A&A, 575, A124
Meisner A. M., Romani R. W., 2010, ApJ, 712, 14
Padovani P., Resconi E., Giommi P., Arsioli B., Chang Y. L., 2016, MNRAS, 457, 3582
Paggi A. et al., 2014, AJ, 147, 112
Paiano S., Landoni M., Falomo R., Scarpa R., Treves A., 2016, MNRAS, 458, 2836
Paiano S., Franceschini A., Stamerra A., 2017a, MNRAS, 468, 4902
Paiano S., Landoni M., Falomo R., Treves A., Scarpa R., Righi C., 2017b, ApJ, 837, 144
Paiano S., Landoni M., Falomo R., Treves A., Scarpa R., 2017c, ApJ, 844, 120
Paiano S., Falomo R., Franceschini A., Treves A., Scarpa R., 2017d, ApJ, 851, 135
Paiano S., Falomo R., Treves A., Scarpa R., 2018, ApJ, 854, L32
Paiano S., Falomo R., Treves A., Franceschini A., Scarpa R., 2019a, ApJ, 871, 162
Paiano S., Falomo R., Treves A., Righi C., Scarpa R., Lindfors E., 2019b, Astron. Telegram, 12802, 1
Perlman E. S. et al., 1996, ApJS, 104, 251
Perlman E. S., Padovani P., Giommi P., Sambruna R., Jones L. R., Tzioumis A., Reynolds J., 1998, AJ, 115, 1253
Piranomonte S., Perri M., Giommi P., Landt H., Padovani P., 2007, A&A, 470, 787
Pita S. et al., 2014, A&A, 565, A12
Plotkin R. M. et al., 2010, AJ, 139, 390
Righi C., Tavecchio F., Inoue S., 2019a, MNRAS, 483, L127
Righi C., Tavecchio F., Pacciani L., 2019b, MNRAS, 484, 2067
Sbarufatti B., Treves A., Falomo R., Heidt J., Kotilainen J., Scarpa R., 2005a, AJ, 129, 559
Sbarufatti B., Treves A., Falomo R., 2005b, ApJ, 635, 173
Sbarufatti B., Treves A., Falomo R., Heidt J., Kotilainen J., Scarpa R., 2006a, AJ, 132, 1
Sbarufatti B., Falomo R., Treves A., Kotilainen J., 2006b, A&A, 457, 35
Sbarufatti B., Ciprini S., Kotilainen J., Decarli R., Treves A., Veronesi A., Falomo R., 2008, AJ, 137, 337S
Sbarufatti B., Ciprini S., Kotilainen J., Decarli R., Treves A., Veronesi A., Falomo R., 2009, AJ, 137, 337
Scarpa R., Urry C. M., Falomo R., Pesce J. E., Treves A., 2000a, ApJ, 532, 740
Scarpa R., Urry C. M., Padovani P., Calzetti D., O'Dowd M., 2000b, ApJ, 544, 258
Schlafly E. F., Finkbeiner D. P., 2011, ApJ, 737, 103
Shaw M. S. et al., 2013, ApJ, 764, 135
Shen Y. et al., 2011, ApJS, 194, 45
Stephen J. B., Bassani L., Landi R., Malizia A., Sguera V., Bazzano A., Masetti N., 2010, MNRAS, 408, 422
Stickel M., Fried J. W., Kuehr H., 1989, A&AS, 80, 103
Stickel M., Padovani P., Urry C. M., Fried J. W., Kuehr H., 1991, ApJ, 374, 431
Stickel M., Fried J. W., Kuehr H., 1993, A&AS, 98, 393
Stickel M., Meisenheimer K., Kuehr H., 1994, A&AS, 105, 211
Stocke J. T., Rector T. A., 1997, ApJ, 489, L17
Stocke J. T., Morris S. L., Gioia I., Maccacaro T., Schild R. E., Wolter A., 1990, ApJ, 348, 141

[4] http://web.oapd.inaf.it/zbllac/

Takeuchi Y., Kataoka J., Maeda K., Takahashi Y., Nakamori T., Tahara M., 2013, ApJS, 208, 25
Tody D., 1986, in Crawford D. L., ed., Proc. SPIE Conf. Ser. Vol. 627, Instrumentation in Astronomy VI. SPIE, Bellingham, p. 733
Tody D., 1993, in Hanisch R. J., Brissenden R. J. V., Barnes J., eds, ASP Conf. Ser. Vol. 52, Astronomical Data Analysis Software and Systems II. Astron. Soc. Pac., San Francisco, p. 173
Urry C. M., Padovani P., 1995, PASP, 107, 803
Urry C. M., Scarpa R., O'Dowd M., Falomo R., Pesce J. E., Treves A., 2000, ApJ, 532, 816
van Dokkum P. G., 2001, PASP, 113, 1420
Voges W. et al., 1999, A&A, 349, 389
Zakamska N. L. et al., 2003, AJ, 126, 2125
Zhu G., Ménard B., 2013, ApJ, 770, 130

SUPPORTING INFORMATION

Supplementary data are available at *MNRAS* online.

Figure 1. Spectra of the unassociated gamma-ray sources obtained at the GTC.

Please note: Oxford University Press is not responsible for the content or functionality of any supporting materials supplied by the authors. Any queries (other than missing material) should be directed to the corresponding author for the article.

This paper has been typeset from a TEX/LATEX file prepared by the author.